

ADP 815 077

2

202000-29-T

AD-A206 540

Technical Report—Study Service Contract

# TASK 1: AUTOMATED ASETS FEASIBILITY

C.D. LAKE

A.J. RIGGS

J.W. SHERMAN

Image Processing Systems Division

MARCH 1989

(Period September 1987—December 1988)

Department of the Air Force  
Armament Division  
Eglin AFB, FL 32542-5320  
F08635-87-C-0074

DTIC  
ELECTE  
S 2 APR 1989 D  
E



ERIM

P.O. Box 8618  
Ann Arbor, MI 48107-8618

This document has been approved  
for public release and under the  
distribution is unlimited.

UNCLASSIFIED

SECURITY CLASSIFICATION OF THIS PAGE

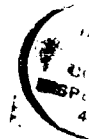
A DA206540

REPORT DOCUMENTATION PAGE				Form Approved OMB No. 0704-0188	
1a REPORT SECURITY CLASSIFICATION Unclassified			1b RESTRICTIVE MARKINGS None		
2a SECURITY CLASSIFICATION AUTHORITY			3 DISTRIBUTION/AVAILABILITY OF REPORT Unlimited		
2b DECLASSIFICATION/DOWNGRADING SCHEDULE					
4 PERFORMING ORGANIZATION REPORT NUMBER(S) 202000-29-T			5 MONITORING ORGANIZATION REPORT NUMBER(S)		
6a NAME OF PERFORMING ORGANIZATION Environmental Research Institute of Michigan		6b OFFICE SYMBOL (if applicable)	7a NAME OF MONITORING ORGANIZATION Department of the Air Force Armament Division		
6c ADDRESS (City, State, and ZIP Code) P.O. Box 8618 Ann Arbor, MI 48107-8618			7b ADDRESS (City, State, and ZIP Code) AD/KRT Eglin AFB, FL 32542-5320		
8a NAME OF FUNDING /SPONSORING ORGANIZATION Department of the Air Force Armament Division		8b OFFICE SYMBOL (if applicable)	9 PROCUREMENT INSTRUMENT IDENTIFICATION NUMBER F08635-87-C-0074		
8c ADDRESS (City, State, and ZIP Code) AD/KRT Eglin AFB, FL 32542-5320			10. SOURCE OF FUNDING NUMBERS		
			PROGRAM ELEMENT NO.	PROJECT NO.	TASK NO.
					WORK UNIT ACCESSION NO.
11. TITLE (Include Security Classification) Task 1: Automated ASETS Feasibility (U)					
12. PERSONAL AUTHOR(S) Charles D. Lake, Alan J. Riggs, James W. Sherman					
13a TYPE OF REPORT Technical		13b. TIME COVERED FROM 9/87 TO 12/88		14. DATE OF REPORT (Year, Month, Day) 1989 March	
15. PAGE COUNT 17					
16 SUPPLEMENTARY NOTATION					
17 COSATI CODES			18. SUBJECT TERMS (Continue on reverse if necessary and identify by block number)		
FIELD	GROUP	SUB-GROUP			
19 ABSTRACT (Continue on reverse if necessary and identify by block number)					
<p>This report addresses the technical issues involved in the analysis of the ASETS image data. Specifically, it outlines issues pertaining to the alignment of data from the CASM instrument collected in the ASETS pod. Actual data was not available at the time this analysis was performed. As such, the topics discussed are fundamental to any effort concerned with correction of this type of data.</p>					
20 DISTRIBUTION/AVAILABILITY OF ABSTRACT <input checked="" type="checkbox"/> UNCLASSIFIED/UNLIMITED <input type="checkbox"/> SAME AS RPT <input type="checkbox"/> DTIC USERS			21 ABSTRACT SECURITY CLASSIFICATION Unclassified		
22a NAME OF RESPONSIBLE INDIVIDUAL James W. Sherman			22b TELEPHONE (Include Area Code) (313) 994-1200 x2829		22c OFFICE SYMBOL

TABLE OF CONTENTS

1.0 INTRODUCTION .....	1
2.0 FACTORS AFFECTING A GEOMETRICALLY CORRECTED STRIP IMAGE .....	3
3.0 ERROR ANALYSIS FRAMEWORK .....	7

Accession For	
NTIS GRA&I	<input checked="" type="checkbox"/>
DTIC TAB	<input type="checkbox"/>
Unannounced	<input type="checkbox"/>
Justification	
By	
Distribution/	
Availability Codes	
Dist	Avail and/or Special
A-1	



## 1.0 INTRODUCTION

This report addresses the technical issues involved in the analysis of the ASETS image data. Specifically, it outlines issues pertaining to the alignment of data from the CASM instrument collected in the ASETS pod. Actual data was not available at the time this analysis was performed. As such, the topics discussed are fundamental to any effort concerned with correction of this type of data.

## 2.0 FACTORS AFFECTING A GEOMETRICALLY CORRECTED STRIP IMAGE

The processing goal is to assemble the data into a single strip of geometrically corrected imagery. For geometric correction to a fixed frame of reference (absolute correction), this entails determining the intersection of the sensor's line-of-sight with the ground. The parameters necessary for this determination are the line-of-sight origin ( $x, y, z$ ), scan angles (depression, sweep), and the terrain elevation (ground  $z$  as a function of ground  $x, y$ ). From this basis of first principles, consideration must be given to the various factors which affect these parameters and their determination. Systematic consideration of these factors typically takes the form of an error analysis. The frame work for an error analysis of the ASETS pod and CASM combination is developed in Section 3. From the eventual error analysis, informed choices can be made regarding measurement accuracy and whether simplifying approximations are acceptable.

Stitching image frames together with imperceptable seams presents several challenges. For the moment, consider the situation in which no geometric alignment is required, i.e., assume perfect alignment and overlap of pixels. Phenomenology in image formation can still result in differing values for many corresponding pixels. The geometry of image formation is perhaps the largest single contributor to pixel differences. For example, obscuration of adjacent objects due to vertical displacement. The CASM sensor operating at 200 meters altitude and nadir orientation will be sensitive to vertical displacements of 3.3 meters for objects near the top or bottom of the frame. At the same altitude, but with a depression angle of 30 degrees, only 87 millimeter vertical displacement of adjacent objects results in a one pixel change in obscuration from the top to the bottom of successive frames. Object movement could also be a factor in pixel differences. The CASM's along-track IFOV at 200 meters altitude is 37 mm, or about 1.5 inches at nadir and 148 mm, about 6 inches at a depression angle of 30 degrees. At a collection rate of 8 frames per second, objects

moving faster than 1 fps, or about 0.7 mph, would be displaced at least 1 pixel in the image data. Given this sensitivity, a modest breeze could result in significant frame to frame differences of objects in the scene. Finally, scene radiance is a function of illumination conditions, scene composition (geometry and reflectance properties), and the observation geometry. Given that these factors do not remain constant between frames, variations in pixel values will persist after corrections are made for alignment of the data.

The next question centers on how frame to frame alignment can be achieved. There are two basic approaches to this problem which can be combined as appropriate. The first approach is to align the data "open loop" by measuring the pointing geometry of the sensor to the accuracy determined by an error analysis. The second approach is to align frames "closed loop" by examining the image data for frame to frame correlations. Selecting the manner in which these approaches are combined involves an analysis of the cost, complexity, and performance trade-offs. We assume that some "closed loop" correction will be necessary. Reasonable bounds on the amount and type of displacement that can be expected after open loop corrections will guide the effort employed in closed loop operations. Closed loop corrections would be based upon contrast differences in the imagery. The number and spatial accuracy of corrections derived from contrast variations needed for achieving the desired system performance can be estimated from the error analysis. Some preliminary observations should be of some interest. Suppose the overlap of the 120 pixels image is between 5% and 10% (6-12 lines of data). For a nadir orientation, this yields 9 to 18 inches of overlap at 200 meters! The numbers quadruple for 30 degree depression angle, but the features are still very small. With only a six to twelve pixel strip for matching, feature matching techniques will be starved for data. Correlation techniques therefore will be very sensitive to the variations in image formation phenomenology.

On the question of measurement accuracy, a common procedure for geometric correction involves a trade-off between sensor position and ground position information. The scenario typically proceeds as follows. The nominal area being imaged is determined from sensor position and scan data. An analyst uses this information to determine what ground data to use for correlation with the imagery, e.g., what map to select. Corresponding points in the ground data and imagery are determined. Using the ground-based positional data, the original imagery is reprojected to a more nearly constant and geometrically correct pixel grid. In short, the ground position information is considered to be more accurate than some of the sensor position and/or scan parameters. The accuracy attained by sensor modelling (FOV, IFOV, scan rate, depression angle, etc.) usually results in ground position data being substituted for sensor position data. Our understanding of ASETS and CASM data is that no ground based positional information will be available. As such, the geometric accuracy of the image data will be solely dependent upon the accuracy of sensor position and modelling parameters.

The line-of-sight origin is typically determined through INS equipment, measurement of the mounting platform, the modelling of the sensor scan characteristics. To minimize flexion and displacement effects, INS equipment is rigidly mounted as close as possible to the sensor. A good understanding of the frequency of perturbations is needed to guide the sampling rate of INS values. In this case, the sensor is mounted on an active pod which is designed to keep orientation errors below one milliradian with a one kilohertz bandwidth. As such, a CASM with a frame time of 22 miliseconds may undergo several positional adjustments in a single frame. Because of this high frequency, the potential exists for coupling effects between sensor data and pod corrections. An error analysis is needed to determine the significance of these effects.

Given an adequate understanding and measurement of the sensor pointing geometry, reprojection of the data to a constant grid size is

possible. For frame to frame alignment, subpixel accuracy is needed for the image seam to be imperceptible. Thus, while it may be possible to correct data to an identical and constant pixel size, there is no guarantee that interframe pixels will be aligned. Under optimal conditions, a single corresponding location from each frame will suffice to shift the images into alignment. More realistically, several corresponding pixels must be determined and their locations fitted to a polynomial. This polynomial is then used to bring one image into alignment with the other. Determination of corresponding locations between frames presents several challenges. In particular, the regions should be small (one pixel), unambiguous in correlation, and sufficient in number and orientation so as to span the dimensional space of the alignment correction.



### 3.0 ERROR ANALYSIS FRAMEWORK

The goal of this section is to develop the equations that relate the errors in pixel location to the various sources of error. By using a small error approximation the covariance of the pixel location errors is computed from the covariance of the sources errors.

The first step is to obtain an expression of the intersection of the sensor's line-of-sight with the ground. This is formed by premultiplying the aircraft INS position relative to a ground coordinate frame by a series of translational and rotational transformations. The resultant intersection point is in ground coordinates.

The aircraft INS position relative to the ground coordinate frames is

$$\bar{I} = x_I(t)\hat{i} + y_I(t)\hat{j} + z_I(t)\hat{k}$$

A new coordinate frame about the INS, aligned with the ground frame, is then:

$$I_0 = \begin{bmatrix} 1 & 0 & 0 & x_I(t) \\ 0 & 1 & 0 & y_I(t) \\ 0 & 0 & 1 & z_I(t) \\ 0 & 0 & 0 & 1 \end{bmatrix}$$

The attitude of this frame varies in time as the airplane pitches ( $\theta_{IY}(t)$ ), yaws ( $\theta_{IZ}(t)$ ), and rolls ( $\theta_{IX}(t)$ ). Frame I is rotated by premultiplying by rotational transformations for each of these motions, and they are:

$$\text{rot } \theta_{IY}(t) = \begin{bmatrix} \cos \theta_{IY}(t) & 0 & \sin \theta_{IY}(t) & 0 \\ 0 & 1 & 0 & 0 \\ -\sin \theta_{IY}(t) & 0 & \cos \theta_{IY}(t) & 0 \\ 0 & 0 & 0 & 1 \end{bmatrix} \quad \text{pitch}$$

$$\text{rot } \theta_{IZ}(t) = \begin{bmatrix} \cos \theta_{IZ}(t) & -\sin \theta_{IZ}(t) & 0 & 0 \\ \sin \theta_{IZ}(t) & \cos \theta_{IZ}(t) & 0 & 0 \\ 0 & 0 & 1 & 0 \\ 0 & 0 & 0 & 1 \end{bmatrix} \quad \text{yaw}$$

$$\text{rot } \theta_{IX}(t) = \begin{bmatrix} 1 & 0 & 0 & 0 \\ 0 & \cos \theta_{IX}(t) & -\sin \theta_{IX}(t) & 0 \\ 0 & \sin \theta_{IX}(t) & \cos \theta_{IX}(t) & 0 \\ 0 & 0 & 0 & 1 \end{bmatrix} \quad \text{roll}$$

The INS frame position as a function of time is thus described by the product:

$$I = \text{rot } \theta_{IY}(t) \text{rot } \theta_{IZ}(t) \text{rot } \theta_{IX}(t) I_0.$$

The gimbal center of the sensor turret is assumed to be positioned rigidly remote from the INS by a vector

$$\bar{R} = x_s \hat{i} + y_s \hat{j} + z_s \hat{k}$$

A frame at the sensor turret gimbal center is obtained by pre-multiplying frame I by a translational transformation as follows:

$$T = \begin{bmatrix} 1 & 0 & 0 & x_s \\ 0 & 1 & 0 & y_s \\ 0 & 0 & 1 & z_s \\ 0 & 0 & 0 & 1 \end{bmatrix} I$$

Frame T, the turret, is servoed in three orthogonal axes: azimuth,  $\theta_{TZ}(t)$ , elevation  $\theta_{TY}(t)$ , and roll  $\theta_{TX}(t)$ . The rotational transformations for these are:

$$\text{rot } \theta_{TZ}(t) = \begin{bmatrix} \cos \theta_{TZ}(t) & -\sin \theta_{TZ}(t) & 0 & 0 \\ \sin \theta_{TZ}(t) & \cos \theta_{TZ}(t) & 0 & 0 \\ 0 & 0 & 1 & 0 \\ 0 & 0 & 0 & 1 \end{bmatrix}$$

$$\text{rot } \theta_{TY}(t) = \begin{bmatrix} \cos \theta_{TY}(t) & 0 & \sin \theta_{TY}(t) & 0 \\ 0 & 1 & 0 & 0 \\ -\sin \theta_{TY}(t) & 0 & \cos \theta_{TY}(t) & 0 \\ 0 & 0 & 0 & 1 \end{bmatrix}$$

$$\text{rot } \theta_{TX}(t) = \begin{bmatrix} 1 & 0 & 0 & 0 \\ 0 & \cos \theta_{TX}(t) & -\sin \theta_{TX}(t) & 0 \\ 0 & \sin \theta_{TX}(t) & \cos \theta_{TX}(t) & 0 \\ 0 & 0 & 0 & 1 \end{bmatrix}$$

The turret frame is premultiplied by these transformations, giving a new turret frame S (for sensor, which is rigidly affixed to the turret)

$$S = \text{rot } \theta_{TX}(t) \text{ rot } \theta_{TY}(t) \text{ rot } \theta_{TZ}(t) T.$$

Within the sensor, a rotating optic sweeps out a scanning IFOV. The axis of rotation is parallel to the turret Z-axis. The sensor frame S is premultiplied by a rotational transformation to yield a frame the X-axis of which is the sensor's line-of-sight.

$$V = \begin{bmatrix} \cos \theta_0(t) & -\sin \theta_0(t) & 0 & 0 \\ \sin \theta_0(t) & \cos \theta_0(t) & 0 & 0 \\ 0 & 0 & 1 & 0 \\ 0 & 0 & 0 & 1 \end{bmatrix} S$$

The intersection of the X-axis of frame V and the ground is the point at which the sensor looks. The ground plane is described by:  $Z = 0$  and has a normal unit vector  $\hat{k}$ .

The origin of frame V is at:  $(V_{14}, V_{24}, V_{34})$ .

The direction of frame V's X-axis is described by the unit vector

$$V_{11}\hat{i} + V_{21}\hat{j} + V_{31}\hat{k}$$

From this information the parametric equations of a line along frame V's X-axis are formed:

$$\frac{x - V_{14}}{V_{11}} = \frac{y - V_{24}}{V_{21}} = \frac{z - V_{34}}{V_{31}} = t$$

Rearranging,

$$x = V_{11}t + V_{14}$$

$$y = V_{21}t + V_{24}$$

$$z = V_{31}t + V_{34}$$

Substituting the equations of the line along frame V's X-axis into the equation for the ground plane:

$$V_{31}t + V_{34} = 0$$

$$t = \frac{-V_{34}}{V_{31}}$$

Substituting this result back into the parametric X-axis line equations yields the intersection of the sensor line-of-sight and the ground plane:

$$V_{11}\left(\frac{-V_{34}}{V_{31}}\right) + V_{14}, V_{21}\left(\frac{-V_{34}}{V_{31}}\right) + V_{24}, V_{31}\left(\frac{-V_{34}}{V_{31}}\right) + V_{34}$$

The actual ground point is some distance  $h$  above the ground plane ( $h$  can be negative, of course). The resulting actual intersection point is displaced in  $x$  and  $y$  of the ground coordinate frame. To find these displacements, the first step is to find the angle between the X-axis and frame  $V$  and the ground plane normal using the dot product:

$$\cos \alpha = \frac{(V_{11}\hat{i} + V_{21}\hat{j} + V_{31}\hat{k}) \cdot \hat{k}}{\sqrt{V_{11}^2 + V_{21}^2 + V_{31}^2}} = V_{31}$$

The angle between the frame  $V$  x-axis and the ground plane itself is  $90^\circ - \alpha$ . The triangle formed by  $90^\circ - \alpha$ ,  $h$ , and the ground plane has a hypotenuse  $\ell$ , where  $\ell$  is the distance along the line-of-sight between the actual ground point and the intersection with the ground plane. It is formed into a vector by multiplying the frame  $V$  X-axis unit vector by  $\ell$ , and this vector is subtracted from the ground plane intersection point.

$$\ell = \frac{h}{V_{31}}$$

$$x' = V_{11}\left(\frac{-V_{34}}{V_{31}}\right) + V_{14} - \frac{h}{V_{31}} V_{11}$$

$$y' = v_{21} \left[ \frac{-v_{34}}{v_{31}} \right] + v_{24} - \frac{h}{v_{31}} v_{21}$$

Rearranging:

$$x' = v_{14} - \frac{v_{11}}{v_{31}} (v_{34} - h)$$

$$y' = v_{24} - \frac{v_{21}}{v_{31}} (v_{34} - h)$$

Calling this result  $\bar{X} = (x', y')$ , the objective is to determine the covariance of  $\bar{X}$  given  $\bar{X}$  is a function of all the variables encountered in the transformation. They form the vector:

$$\bar{p} = [h(t), \theta_o(t), \theta_{TX}(t), \theta_{TY}(t), \theta_{TX}(t), \theta_{IY}(t), \theta_{IZ}(t), \\ \theta_{IX}(t), x_I(t), y_I(t), z_I(t)]$$

Starting with:

$$\text{Cov } \bar{X}(\bar{p}) = E \left\{ \left[ \bar{X}(\bar{p}) - E\{\bar{X}(\bar{p})\} \right] \left[ \bar{X}(\bar{p}) - E\{\bar{X}(\bar{p})\} \right]^T \right\}$$

expand  $\bar{X}(\bar{p})$  in a Taylor series:

$$\bar{X}(\bar{p}) = \bar{X}(\bar{p}) \Big|_{\bar{p}=\bar{p}_0} + \nabla \bar{p} [\bar{X}(\bar{p})]^T \Big|_{\bar{p}=\bar{p}_0} [\bar{p} - \bar{p}_0] + \dots \text{higher order terms} \\ \text{(assume negligible)}$$

the choosing  $\bar{p}_0 = E\{\bar{p}\}$

$$E\{\bar{X}(\bar{p})\} = \bar{X}(\bar{p}_0) + \nabla \bar{p} [\bar{X}(\bar{p})]^T \Big|_{\bar{p}=\bar{p}_0} E[\bar{p} - \bar{p}_0]$$

$$E\{\bar{X}(\bar{p})\} = \bar{X}(\bar{p}_0)$$

Substituting this result into the equation for Cov  $\bar{X}(\bar{p})$ :

$$\begin{aligned} \text{Cov } \bar{X}(\bar{p}) &= E\left\{\left[\bar{X}(\bar{p}_0) + \nabla\bar{p}[\bar{X}(\bar{p})]\right]^T \bigg|_{\bar{p}=\bar{p}_0} [\bar{p} - \bar{p}_0] - \bar{X}(\bar{p}_0)\right. \\ &\quad \left. \left[\nabla\bar{p}[\bar{X}(\bar{p})]^T [\bar{p} - \bar{p}_0]\right]^T\right\} \\ &= E\left\{\nabla\bar{p} \left[\bar{X}(\bar{p}_0)\right]^T [\bar{p} - \bar{p}_0] [\bar{p} - \bar{p}_0]^T \nabla\bar{p} \bar{X}(\bar{p}_0)\right\} \\ &= \nabla\bar{p} \left[\bar{X}(\bar{p}_0)\right]^T \bigg|_{\bar{p}=\bar{p}_0} E\left\{[\bar{p} - \bar{p}_0] [\bar{p} - \bar{p}_0]^T\right\} \nabla\bar{p} [\bar{X}(\bar{p})] \bigg|_{\bar{p}=\bar{p}_0} \end{aligned}$$

Next, each of the components of the above equation are formed.

$$\begin{aligned} \nabla\bar{p}[\bar{X}(\bar{p})] &= \nabla\bar{p} \begin{bmatrix} v_{14} \\ v_{24} \end{bmatrix} - \nabla\bar{p} \begin{bmatrix} v_{11}v_{31}^{-1}(v_{34} - h) \\ v_{21}v_{31}^{-1}(v_{34} - h) \end{bmatrix} \\ &= \begin{bmatrix} \nabla\bar{p} v_{14} \\ \nabla\bar{p} v_{24} \end{bmatrix} - \begin{bmatrix} (\nabla\bar{p} v_{11})v_{31}^{-1}(v_{34} - h) - v_{11}(v_{34} - h) \\ (\nabla\bar{p} v_{21})v_{31}^{-1}(v_{34} - h) - v_{21}(v_{34} - h) \end{bmatrix} \\ &\quad \begin{bmatrix} v_{31}^{-2} \nabla\bar{p} v_{31} + v_{11}v_{31}^{-1} \nabla\bar{p} v_{34} - v_{11}v_{31}^{-1} \nabla\bar{p} h \\ v_{31}^{-2} \nabla\bar{p} v_{31} + v_{21}v_{31}^{-1} \nabla\bar{p} v_{34} - v_{21}v_{31}^{-1} \nabla\bar{p} h \end{bmatrix} \end{aligned}$$

$$\begin{aligned}
 &= \begin{bmatrix} \nabla \bar{p} v_{14k} \\ \nabla \bar{p} v_{24k} \end{bmatrix} - \begin{bmatrix} \nabla \bar{p} v_{11k} v_{31}^{-1} (v_{34} - h) - v_{11} (v_{34} - h) v_{31}^{-2} \nabla \bar{p} v_{31k} \\ \nabla \bar{p} v_{21k} v_{31}^{-1} (v_{34} - h) - v_{21} (v_{34} - h) v_{31}^{-2} \nabla \bar{p} v_{31k} \\ + v_{11} v_{31}^{-1} \nabla \bar{p} v_{34k} - v_{11} v_{31}^{-1} (1 \ 0 \ 0 \ 0 \ 0 \ 0 \ 0 \ 0 \ 0 \ 0 \ 0) \\ + v_{21} v_{31}^{-1} \nabla \bar{p} v_{34k} - v_{21} v_{31}^{-1} (1 \ 0 \ 0 \ 0 \ 0 \ 0 \ 0 \ 0 \ 0 \ 0 \ 0) \end{bmatrix}
 \end{aligned}$$

where the  $\nabla \bar{p} v_{ijk}$  terms are obtained by taking the partial derivative of the  $V$  matrix with respect to all the elements of  $\bar{p}$ . Recall that matrix  $V$  is the product of nine matrices, and  $\bar{p}$  is a vector of eleven elements.

$$P_1 = h(t), P_2 = \theta_0(t), P_3 = \theta_{TZ}(t), P_4 = \theta_{TY}(t), P_5 = \theta_{TX}(t),$$

$$P_6 = \theta_{IY}(t), P_8 = \theta_{IX}(t), P_9 = x_I(t), P_{10} = y_I(t), P_{11} = z_I(t)$$

$$\begin{aligned}
 M_1 &= \begin{bmatrix} \cos \theta_0(t) & -\sin \theta_0(t) & 0 & 0 \\ \sin \theta_0(t) & \cos \theta_0(t) & 0 & 0 \\ 0 & 0 & 1 & 0 \\ 0 & 0 & 0 & 1 \end{bmatrix} & \frac{\partial M_1}{\partial p_2} &= \begin{bmatrix} -\sin \theta_0(t) & -\cos \theta_0(t) & 0 & 0 \\ \cos \theta_0(t) & -\sin \theta_0(t) & 0 & 0 \\ 0 & 0 & 0 & 0 \\ 0 & 0 & 0 & 0 \end{bmatrix} \\
 M_2 &= \begin{bmatrix} \cos \theta_{TZ}(t) & -\sin \theta_{TZ}(t) & 0 & 0 \\ \sin \theta_{TZ}(t) & \cos \theta_{TZ}(t) & 0 & 0 \\ 0 & 0 & 1 & 0 \\ 0 & 0 & 0 & 1 \end{bmatrix} & \frac{\partial M_2}{\partial p_3} &= \begin{bmatrix} -\sin \theta_{TZ}(t) & -\cos \theta_{TZ}(t) & 0 & 0 \\ \cos \theta_{TZ}(t) & -\sin \theta_{TZ}(t) & 0 & 0 \\ 0 & 0 & 0 & 0 \\ 0 & 0 & 0 & 0 \end{bmatrix} \\
 M_3 &= \begin{bmatrix} \cos \theta_{TY}(t) & 0 & \sin \theta_{TY}(t) & 0 \\ 0 & 1 & 0 & 0 \\ -\sin \theta_{TY}(t) & 0 & \cos \theta_{TY}(t) & 0 \\ 0 & 0 & 0 & 1 \end{bmatrix} & \frac{\partial M_3}{\partial p_4} &= \begin{bmatrix} -\sin \theta_{TY}(t) & 0 & \cos \theta_{TY}(t) & 0 \\ 0 & 0 & 0 & 0 \\ -\cos \theta_{TY}(t) & 0 & -\sin \theta_{TY}(t) & 0 \\ 0 & 0 & 0 & 0 \end{bmatrix}
 \end{aligned}$$



$$M_4 = \begin{bmatrix} 1 & 0 & 0 & 0 \\ 0 & \cos \theta_{TX}(t) & -\sin \theta_{TX}(t) & 0 \\ 0 & \sin \theta_{TX}(t) & \cos \theta_{TX}(t) & 0 \\ 0 & 0 & 0 & 1 \end{bmatrix}$$

$$\frac{\partial M_4}{\partial p_5} = \begin{bmatrix} 0 & 0 & 0 & 0 \\ 0 & -\sin \theta_{TX}(t) & -\cos \theta_{TX}(t) & 0 \\ 0 & \cos \theta_{TX}(t) & -\sin \theta_{TX}(t) & 0 \\ 0 & 0 & 0 & 0 \end{bmatrix}$$

$$M_5 = \begin{bmatrix} 1 & 0 & 0 & x_s \\ 0 & 1 & 0 & y_s \\ 0 & 0 & 1 & z_s \\ 0 & 0 & 0 & 1 \end{bmatrix}$$

$$M_6 = \begin{bmatrix} \cos \theta_{IY}(t) & 0 & \sin \theta_{IY}(t) & 0 \\ 0 & 1 & 0 & 1 \\ -\sin \theta_{IY}(t) & 0 & \cos \theta_{IY}(t) & 0 \\ 0 & 0 & 0 & 1 \end{bmatrix}$$

$$\frac{\partial M_6}{\partial p_6} = \begin{bmatrix} -\sin \theta_{IY}(t) & 0 & \cos \theta_{IY}(t) & 0 \\ 0 & 0 & 0 & 0 \\ -\cos \theta_{IY}(t) & 0 & -\sin \theta_{IY}(t) & 0 \\ 0 & 0 & 0 & 0 \end{bmatrix}$$

$$M_7 = \begin{bmatrix} \cos \theta_{IZ}(t) & -\sin \theta_{IZ}(t) & 0 & 0 \\ \sin \theta_{IZ}(t) & \cos \theta_{IZ}(t) & 0 & 0 \\ 0 & 0 & 1 & 0 \\ 0 & 0 & 0 & 1 \end{bmatrix}$$

$$\frac{\partial M_7}{\partial p_7} = \begin{bmatrix} -\sin \theta_{IZ}(t) & -\cos \theta_{IZ}(t) & 0 & 0 \\ \cos \theta_{IZ}(t) & -\sin \theta_{IZ}(t) & 0 & 0 \\ 0 & 0 & 0 & 0 \\ 0 & 0 & 0 & 0 \end{bmatrix}$$

$$M_8 = \begin{bmatrix} 1 & 0 & 0 & 0 \\ 0 & \cos \theta_{IX}(t) & -\sin \theta_{IX}(t) & 0 \\ 0 & \sin \theta_{IX}(t) & \cos \theta_{IX}(t) & 0 \\ 0 & 0 & 0 & 1 \end{bmatrix}$$

$$\frac{\partial M_8}{\partial p_8} = \begin{bmatrix} 0 & 0 & 0 & 0 \\ 0 & -\sin \theta_{IX}(t) & -\cos \theta_{IX}(t) & 0 \\ 0 & \cos \theta_{IX}(t) & -\sin \theta_{IX}(t) & 0 \\ 0 & 0 & 0 & 0 \end{bmatrix}$$

$$M_9 = \begin{bmatrix} 1 & 0 & 0 & x_I(t) \\ 0 & 1 & 0 & y_I(t) \\ 0 & 0 & 1 & z_I(t) \\ 0 & 0 & 0 & 1 \end{bmatrix} \quad \frac{\partial M_9}{\partial p_9} = \begin{bmatrix} 0 & 0 & 0 & 1 \\ 0 & 0 & 0 & 0 \\ 0 & 0 & 0 & 0 \\ 0 & 0 & 0 & 0 \end{bmatrix}$$

$$\frac{\partial M_9}{\partial p_{10}} = \begin{bmatrix} 0 & 0 & 0 & 0 \\ 0 & 0 & 0 & 1 \\ 0 & 0 & 0 & 0 \\ 0 & 0 & 0 & 0 \end{bmatrix} \quad \frac{\partial M_9}{\partial p_{11}} = \begin{bmatrix} 0 & 0 & 0 & 0 \\ 0 & 0 & 0 & 0 \\ 0 & 0 & 0 & 1 \\ 0 & 0 & 0 & 0 \end{bmatrix}$$

All the other partial derivatives of the M's with respect to any of the p's are all zeroes. Using the above matrices,

$$\nabla \bar{p} V^T = \begin{bmatrix} \frac{\partial V}{\partial p_1} \\ \vdots \\ \frac{\partial V}{\partial p_{11}} \end{bmatrix}^T = \begin{bmatrix} \sum_{j=1}^{11} M_1 \dots M_{j-1} \left[ \frac{\partial M_j}{\partial p_1} \right] M_{j+1} \dots M_9 & k=1 \\ \vdots & \vdots \\ \sum_{j=1}^{11} M_1 \dots M_{j-1} \left[ \frac{\partial M_j}{\partial p_{11}} \right] M_{j+1} \dots M_9 & k=11 \end{bmatrix}^T$$

$\nabla \bar{p} V^T$  is a  $[44 \times 4]$  matrix that has been triple indexed as an  $[11 \times 1]$  where each of the eleven elements is a  $[4 \times 4]$ . The equation for  $\nabla \bar{p}^T \bar{X}(\bar{p})$  on page 10 then uses elements of  $\nabla \bar{p} V^T$  as well as elements of  $V$ .

The next component of Cov  $X(p)$  to be formed is

$$E \left\{ \left[ \bar{p} - \bar{p}_0 \right] \left[ \bar{p} - \bar{p}_0 \right]^T \right\}.$$

Because the interest is in how the variables of  $\bar{p}$  correlate in time, the above will be written as:

$$E\left\{\left[\Delta\bar{p}(t_1)\right]\left[\Delta\bar{p}(t_2)\right]^T\right\} = \left[E\left\{\Delta p_i(t_1)\Delta p_j(t_2)\right\}\right].$$

This results in a  $[11 \times 11]$  matrix that is strongly diagonally dominant and symmetric. Values for the nonzero elements of this matrix are then to be taken from models of the actual random processes describing the behavior of the  $\bar{p}$  variables with time.

The final result,  $\text{Cov } \bar{X}(\bar{p})$ , is dimensionally:

$$\begin{aligned}\text{Cov } X(p) &= [2 \times 11] \begin{bmatrix} 11 \times 11 \end{bmatrix} \begin{bmatrix} 11 \\ x \\ 2 \end{bmatrix} \\ &= [2 \times 2]\end{aligned}$$